

Towards Trapped-Ion Thermometry Using Cavity-Based EIT

Abhijit Kundu,¹ Vijay Bhatt,¹ and Arijit Sharma^{1,2,*}

¹*Department of Physics, Indian Institute of Technology Tirupati, Yerpedu-517619, Andhra Pradesh, India.*

²*Center for Atomic, Molecular, and Optical Sciences and Technologies,
Indian Institute of Technology Tirupati, Yerpedu-517619, Andhra Pradesh, India.*

(Dated: March 10, 2026)

We present a technique for measuring ion temperature using cavity-based electromagnetically induced transparency (EIT) applicable for cavity quantum electrodynamics (QED) systems in the strong coupling regime. This method enables efficient extraction of the ion's phonon occupation number following sub-Doppler cooling close to the motional ground state. The proposed method relies on monitoring the cavity probe transmission while scanning the probe laser frequency to establish cavity-induced EIT using the control beam, significantly simplifying the measurement procedure. We establish a theoretical model that demonstrates the influence of the thermal state of the trapped ion vis-à-vis the EIT linewidth measured. We show through numerical simulations how the cavity-induced EIT transmission may be used as a thermometry tool to deduce the ion temperature as well as the motional state of the ion in the sub-Doppler cooling regime, even for systems that are in the weak coupling regime. The current method can only be used for operation in the resolved-sideband regime, where individual motional states can be selectively addressed for all relevant transitions either by selecting appropriate energy levels for the three-level system or by employing strong confinement with high secular frequencies ($\sim 10MHz$).

I. INTRODUCTION

Trapped ions offer a well-controlled platform for precision metrology, cavity quantum electrodynamics (QED), and quantum information processing due to their long coherence time and exceptional degree of experimental controllability [1–4].

With successful demonstrations across a broad range of ion species and trap architectures, resolved sideband cooling has emerged as the standard technique for preparing trapped ions close to the motional ground state [5–7]. Achieving and confirming near-ground-state cooling is essential, since even a small residual motional excitation can degrade coherence and reduce the fidelity of quantum operations [7, 8]. For this reason, accurate thermometry after sideband cooling is crucial for describing cooling performance and validating subsequent quantum operations. After compensation of excess micromotion, it is possible to characterize the motion of a trapped ion in a radio-frequency Paul trap [7]. Ion temperature is directly determined by a discrete phonon occupation number that characterizes the motional state.

Determining this phonon occupation provides a crucial benchmark for coherent quantum operations and enables a direct evaluation of the ions' thermal state [1, 7, 9].

A variety of techniques have been developed to deduce the motional occupation of trapped ions [9–11]. The most popular method is resolved sideband thermometry, which assumes a thermal motional distribution and uses the ratio of red to blue sideband transition strengths to estimate the mean phonon number [5, 12]. More generally, reconstruction techniques that do not strictly rely on thermal assumptions are made possible by extracting phonon distribution information from Rabi oscillations in carrier and sideband transitions [9–11]. These methods are well known and typically require precise internal-state preparation and the detection of projective states.

Over the past few decades, following the seminal works of Kimble [13], Haroche [14] and Rempe [15], there has been growing interest in cavity quantum electrodynamics with trapped ions due to its potential for the realization of scalable quantum networks, enhanced light-matter coupling, and effective ion-photon interfaces for quantum information processing schemes and applications [16–22].

* arijit@iittp.ac.in

Interference-based phenomena such as cavity-assisted electromagnetic-induced transparency (EIT) are made possible by the presence of an optical cavity, which alters the interaction between the ion and the electromagnetic field. Since its discovery, EIT [23] has made it possible for a wide range of coherent optical control applications, such as slow light in atomic medium [24], quantum memory [25], laser cooling [26], precision spectroscopy, and sensing [16].

Cavity-based EIT has been studied in a number of regimes to enable features such as narrowing of the cavity linewidth and enhanced optical nonlinearities [19, 20, 27]. A key feature of cavity-induced EIT is its sensitivity to decoherence mechanisms in the coupled ion-cavity system. Coupling to vibrational sidebands causes phonon-dependent dephasing of the effective Λ -type system in the presence of motional excitation, changing the coherence, and altering the EIT interference [26, 28]. The cavity-EIT transparency window is thus systematically expanded by thermal phonons. Thermally induced fluctuations alter the effective decoherence rates in the presence of motional excitation which affects the EIT transparency features' width and shape. This dependence suggests that the cavity-EIT can serve as an indirect probe of the ion's motional temperature.

In this article, we theoretically investigate a cavity-enhanced thermometry scheme for trapped ions that exploits the phonon-induced modification of cavity-induced EIT. We consider a Λ -type trapped ion cavity-QED system in which an auxiliary internal transition of the ion is driven by a coupling (control) laser and the cavity mode is interacted with a weak probe field. By including vibrational sidebands and the ion's motion coupled to a thermal reservoir in a Λ -type ion-cavity setup, we demonstrate that the phonon occupation of the trapped ion modifies the cavity EIT linewidth in a systematic manner. This dependence can be used as a direct probe of the mean phonon number by tuning the coupling field to motional sideband transitions. Thus, the suggested method offers

a cavity-compatible thermometry technique that does not depend on projective state detection after sideband cooling. Our theoretical framework establishes a direct link between measurable modification of the cavity-EIT resonance and motional decoherence induced by thermal phonon. The proposed approach provides an experimentally feasible alternative to conventional sideband thermometry in trapped-ion cavity-QED systems.

We show that the coupling laser causes a phonon number-dependent change in the effective Rabi frequency when it is tuned to a motional sideband transition. This results in a systematic and temperature-dependent broadening of the cavity-EIT feature. We determine a quantitative relationship between the measured cavity-EIT linewidth and the ion temperature by numerically solving the complete open-system dynamics, which includes cavity loss, spontaneous emission, and phonon damping caused by a thermal reservoir. Our results indicate that this technique allows for precise thermometry in the resolved-sideband and sub-Doppler regimes and can be expanded to parameter regimes that are consistent with experimentally realized strong coupling ion-cavity systems[19–22].

We subsequently extend the model to the multi-ion system by modifying the atom-cavity interaction Hamiltonian to include a summation over all ions coupled to the same cavity mode. In this formulation, each ion interacts with the cavity field identically, and the collective response of the ion ensemble naturally emerges from the full many-body master equation. This approach allows us to examine thermometry in regimes where the cavity response is improved by the collective light-matter interaction and the single-ion coupling strength to the intracavity field places the system in the weak coupling regime.

To summarize, we establish a direct link between motional decoherence and cavity transmission, and propose a cavity-compatible

minimally invasive thermometry technique for trapped ions through modeling and simulations. Beyond thermometry, the demonstrated sensitivity of cavity-EIT to the motional state of the ion creates new opportunities for studying measurement-induced back-action in cavity-QED systems and for monitoring of thermal dynamics.

The article is organized as follows: In section II, we present the theoretical model and Hamiltonian, including the treatment of ion motion and dissipative processes. In section III, numerical results for linewidth extraction and cavity transmission are shown. The section IV examines how phonons affect the cavity-EIT spectrum. The analysis of ion temperature and the role of thermalization dynamics are discussed in section V. The discussion then extends to multi-ion cavity-QED systems operating in the weak single-ion coupling regime in section VI, where we demonstrate that thermometry is made possible even in cases where individual coupling strengths are small through collective enhancement. section VII further investigates the applicability of the proposed method to systems with large excited state decay rates. We show conclusively that thermometry remains feasible under realistic experimental conditions. We present a realistic experimental realization roadmap in section VIII covering parameter regimes compatible with existing ion-cavity platform trap requirements and viable cavity configurations. Finally, a summary of the key results and concluding remarks are given in section IX.

II. THEORY AND MODEL

Cavity-based EIT systems have been extensively studied over the past two decades [19, 20, 27, 29–33]. These studies demonstrate that the cavity output can be effectively controlled by several key parameters, including the atom-cavity coupling strength (g), control field Rabi frequency (Ω_c), and the cavity decay rate (κ). Among these parameters, the control field intensity, Ω_c , represents an experimentally

accessible degree of freedom, whereas the others are primarily defined by the cavity geometry, mirror reflectivity, and the choice of atomic energy levels. As a result, parameters such as g and κ cannot be easily tuned under typical experimental constraints, whereas Ω_c can be easily modified by tweaking the laser power. As the control field intensity Ω_c increases, the full width at half maximum (FWHM) of the EIT resonance also increases significantly, typically by ≈ 10 kHz. This dependence forms the basis of the proposed thermometry scheme.

For the purpose of ion thermometry, it is essential to include the vibrational levels associated with each relevant electronic energy level. Addressing these vibrational states requires operation in the resolved-sideband regime ($\gamma \ll \omega_{sec}$) [1, 34], where the splitting between adjacent vibrational levels, $\hbar\omega_{sec}$, exceeds the natural linewidth of the corresponding transition, 2γ . Here, γ denotes the spontaneous decay rate of the transition and ω_{sec} represents the secular frequency of the trapped ion.

Henceforth, a transition between two energy levels refers to a transition between their corresponding vibrational states. The allowed transitions can be classified into three main types: the carrier transition, the blue sideband (BSB) transition, and the red sideband (RSB) transition, corresponding to $\Delta n = 0$ and $\Delta n = \pm 1$, respectively. When sideband transitions are addressed, the vibrational level occupancy, n , certainly influences the ion-field coupling strength. Consequently, the Rabi frequencies for the RSB and BSB transitions get modified as [1],

$$\begin{aligned}\Omega_{BSB} &= \Omega_0 \sqrt{n+1}, \\ \Omega_{RSB} &= \Omega_0 \sqrt{n}.\end{aligned}\tag{1}$$

Unlike the previous case, the Rabi frequency (Ω_0) remains unchanged for the carrier transition. Thus, when the control laser is tuned to a sideband transition (BSB or RSB), the effect of the phonon occupancy, n , becomes evident in the EIT linewidth through its influence on the Rabi frequency, Ω_c . In other words, variations in the EIT linewidth provide an estimate of

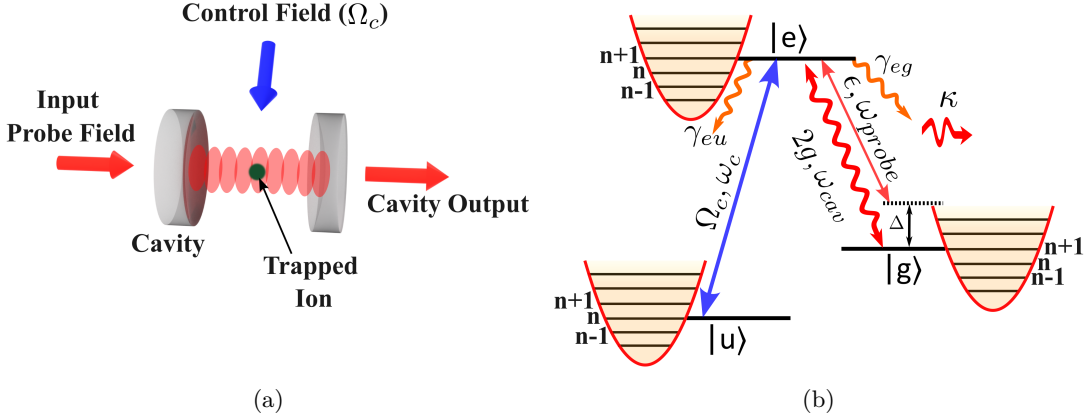


FIG. 1: (a) Schematic of the cavity-based electromagnetically induced transparency (EIT) configuration, where a trapped ion interacts with a single cavity mode. (b) Energy-level diagram of the cavity-EIT scheme including vibrational states. The coupling laser drives the $|u\rangle \rightarrow |e\rangle$ transition with the addition of one vibrational quantum, while spontaneous decay to $|g\rangle$ preserves the vibrational level. The probe field and cavity mode couple the $|e\rangle$ and $|g\rangle$ states.

changes in the ion's vibrational occupancy. Motivated by this correlation, we define a systematic approach via numerical simulations for determining the ion temperature via phonon occupancy.

We consider a Λ -type three-level system confined inside a high-finesse optical cavity. The states are considered to be coupled with vibrational states, denoted by $|u, n\rangle$, $|e, n+1\rangle$, and $|g, n\rangle$. The cavity mode couples to the atomic transition $|g, n+1\rangle \leftrightarrow |e, n+1\rangle$ with coupling strength g , while a classical control laser couples the transition $|u, n\rangle \leftrightarrow |e, n+1\rangle$ by a change in single quanta of the phonon mode with Rabi frequency Ω_c (see Figure 1b). A weak input probe field of amplitude ϵ and frequency ω_{probe} is applied at probe detuning (Δ). To obtain the cavity output, the Δ is scanned on both side of the cavity resonance. The spontaneous decay rates from level $|e, n+1\rangle \rightarrow |u, n+1\rangle$ and $|e, n+1\rangle \rightarrow |g, n+1\rangle$ are γ_{eu} and, γ_{eg} respectively.

We operate in the Lamb-Dicke regime ($\eta \ll 1$), where the control laser and ion's motion can be expanded to first order in the Lamb-Dicke parameter η . Operators b and b^\dagger describe phonon-assisted transitions, achieved by tuning

the coupling laser to the first motional sideband of the $|u\rangle \leftrightarrow |e\rangle$ transition [1].

In the rotating frame defined by the probe frequency ω_{probe} , the dynamics of the system can be described by the following time-independent Hamiltonian under the electric dipole and rotating-wave approximation (RWA) (with $\hbar = 1$):

$$H = \Delta_p \sigma_{gg} - \Delta_p a^\dagger a + g (a^\dagger \sigma_{ge} + a \sigma_{eg}) + \eta \Omega_c (\sigma_{eu} b^\dagger + \sigma_{ue} b) + \epsilon (a^\dagger + a). \quad (2)$$

Here, $\sigma_{ij} = |i\rangle \langle j|$ are the ionic transition operators. The detuning parameter $\Delta_p = \omega_{probe} - \omega_{31}$ represents the frequency mismatch between the probe laser and the atomic transition $|g, n+1\rangle \leftrightarrow |e, n+1\rangle$.

The first term of the Hamiltonian in Equation 2 describes the energy of the atomic state $|g, n+1\rangle$ in the rotating frame, while the second term corresponds to the energy of the cavity photons. The cavity field is described by photon annihilation (a) and creation (a^\dagger) operators.

The third term of the Hamiltonian in Equa-

tion 2 accounts for the coherent interaction between the cavity field and the atomic transition $|g, n+1\rangle \leftrightarrow |e, n+1\rangle$. The fourth term describes the interaction between the atomic transition $|e, n+1\rangle \leftrightarrow |u, n+1\rangle$ and the vibrational mode of the ion, mediated by the control laser. Here, b and b^\dagger are the phonon annihilation and creation operators respectively. The last term represents the coherent drive applied to the cavity field by the pump laser.

The open dynamics follow the Lindblad master equation [35],

$$\begin{aligned} \frac{d\rho}{dt} = & -i[H, \rho] + \kappa (2a\rho a^\dagger - a^\dagger a\rho - \rho a^\dagger a) \\ & + \gamma_{eu} (2\sigma_{ue}\rho\sigma_{eu} - \sigma_{ee}\rho - \rho\sigma_{ee}) \\ & + \gamma_{eg} (2\sigma_{ge}\rho\sigma_{eg} - \sigma_{ee}\rho - \rho\sigma_{ee}) \quad (3) \\ & + \gamma_b(n_{th} + 1) (2b\rho b^\dagger - b^\dagger b\rho - \rho b^\dagger b) \\ & + \gamma_b n_{th} (2b^\dagger\rho b - bb^\dagger\rho - \rho bb^\dagger) \end{aligned}$$

where ρ represents the density matrix of the ion-cavity system and κ denotes the decay rate of the cavity field.

γ_{eg} and γ_{eu} represent the spontaneous decay rate from state $|e\rangle$ to state $|g\rangle$ and $|u\rangle$. γ_b is the phonon damping rate and n_{th} denotes the mean thermal phonon number at equilibrium.

The average phonon number (\bar{n}) is related to the temperature of the ion as,

$$\bar{n} = \frac{1}{\exp(\hbar\omega_{osc}/k_bT) - 1} \quad (4)$$

The phonon states are inherent to damping due to fluctuating electric field noise present in real ion trap. To account for this scenario, we considered the trapped ion system such that it is coupled to a thermal bath. Fluctuating electric-field noise induces phonon exchange between the ion and the reservoir, driving the system toward thermal equilibrium [8].

The rate equation for the phonons can be derived as [8],

$$\dot{\bar{n}}(t) = -\gamma_b \bar{n}(t) + \gamma_b n_{th} \quad (5)$$

so close to the ground state ($\bar{n} = 0$), $\dot{\bar{n}}(t) = \gamma_b n_{th}$. This gives an initial estimation of the heating rate of the ion. Equation 5, also shows that if a long time interval is taken, i.e., at equilibrium, $\bar{n}_{eq} = n_{th}$. So, determining the value of n_{th} allows us to estimate the ion's temperature owing to Equation 4.

III. ANALYSIS OF TRANSMISSION IN CAVITY-EIT

To study the system dynamics, we numerically solve the master equation (Equation 3) using the Hamiltonian given in Equation 2 for a single ion strongly coupled to the intracavity field. The probe-field detuning is varied across the cavity resonance while keeping the other system parameters fixed. The steady-state density matrix is obtained for each value of the probe detuning.

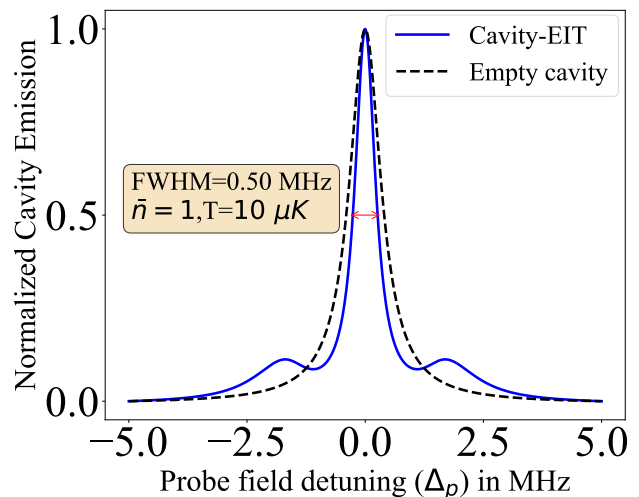


FIG. 2: Simulated cavity-EIT transmission spectrum for $\kappa = 0.4$ MHz, $g = 3\kappa$, $\gamma_{eg} = \gamma_{eu} = \kappa$, $\langle n \rangle = 1$, and $\gamma_b = 0.25\kappa$. The observed linewidth (0.55 MHz) is narrower than the empty cavity linewidth $2\kappa = 0.8$ MHz. The vacuum Rabi splitting peaks occur at $\pm\sqrt{g^2 + \Omega_c^2} = \pm 1.56$ MHz.

From the steady-state solution, the photon population inside the cavity is extracted by

evaluating the expectation value of the photon number operator, $\langle a^\dagger a \rangle$. The steady-state intracavity photon number, which is proportional to the output field leaking through the cavity mirrors, is then used to calculate the transmission spectrum. Figure 2) shows the resulting transmission profile. This spectrum exhibits the characteristic features of previously reported cavity-EIT systems [19, 20, 27, 36].

The cavity linewidth is observed to be narrower than that of an empty cavity, and the vacuum Rabi splitting peaks appear at $\Delta = \pm\sqrt{g^2 + \Omega_c^2}$. For all simulations presented in this work, unless otherwise stated, the system parameters are fixed as follows. All quantities are normalized with respect to the cavity decay rate, κ , which is taken to be 0.4 MHz, a typical value for a high-finesse cavity. The coupling-field Rabi frequency, Ω_c , is set to 2.5κ , while the atom-cavity coupling strength, g , is chosen as 3κ . The decay rates from the excited states, γ_{ge} and γ_{ue} , are taken to be equal to κ . In addition, motional-state decoherence is included to account for unwanted heating or cooling of the ion arising from phase noise and radiative fluctuations present in realistic ion traps. To model this effect, a weak coupling between the motional state and the environment is introduced, characterized by a coupling constant $\gamma_b \approx 0.25\kappa$.

IV. EFFECT OF THERMAL STATE ON CAVITY EIT LINEWIDTH

The usual cavity-EIT formalism discussed and reviewed through multiple theoretical approaches [37–39] as well as experimental investigations [32, 40] till date has not explicitly considered the ion’s motional state in the realization of the cavity-induced EIT phenomenon. This inherently makes an assumption that the ion is fixed in space and the effect of ion thermalization does not affect the cavity-EIT output. When the ion’s motion is not considered for cavity-based

EIT, the Hamiltonian is simplified to,

$$H_{\text{EIT}} = \Delta_p \sigma_{gg} - \Delta_p a^\dagger a + g (a^\dagger \sigma_{ge} + \sigma_{eg} a) + \Omega_c (\sigma_{ue} + \sigma_{eu}) + \varepsilon (a^\dagger + a). \quad (6)$$

where the different terms have their usual meaning as described in section II. We refer to this formalism as non-thermal and the Hamiltonian given in Equation 6, the non-thermal cavity-EIT Hamiltonian. The output of the cavity is traced from the average of the photon number operator with the variation of the probe field detuning. The same cavity transmission can also be analytically calculated from the expression[41],

$$T = \frac{\kappa^2}{|(\Delta_p + i\kappa) - g^2 N \chi|^2} \quad (7)$$

where,

$$\chi = g^2 N \frac{\Delta_p}{(\Delta_p + i(\gamma_{eu} + \gamma_{eg})\Delta_p - \frac{1}{4}\Omega_c^2)} \quad (8)$$

The linewidth depends on the effective Rabi coupling, Ω_c , exhibiting power-broadening behavior. In Figure 3a, the relationship between the effective Rabi coupling and the cavity-EIT linewidth is shown using the analytical expression.

When the motional states are incorporated into the Hamiltonian (Equation 10), it encompasses a more general description of a trapped ion, the cavity-EIT linewidth deviates from the non-thermal case. As the temperature increases, the thermal nature of the ion leads to a higher motional occupancy. This increase in motional occupation modifies the cavity-EIT linewidth by changing Ω_c , as discussed in detail in section II.

To compare the cavity-induced EIT linewidths in the thermal (when motional states are included) and non-thermal (when motional states are not considered) cases, we perform simulations for both scenarios using the same values of Ω_c as those employed in the analytical plot in Figure 3a. The thermal simulations are carried out over a range of temperatures to capture the

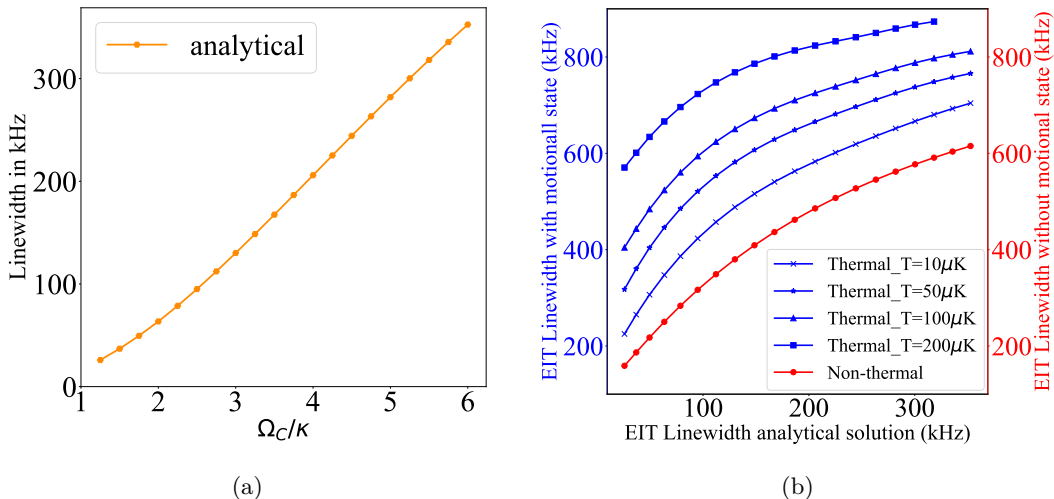


FIG. 3: (a) Cavity-EIT linewidth from analytical expression as a function of control field Rabi frequency. (b) Comparison of linewidth without considering motional state vs with motional state for different temperatures of ion. The parameters for the plots chosen as follows, $\kappa = 0.4\text{MHz}$, $g = 3\kappa$, $\gamma_{eg} = \gamma_{eu} = \kappa$, $\gamma_b = 0.04\kappa$.

dependence of the cavity-induced EIT linewidth on the ion temperature. In Figure 3b, the thermal and non-thermal linewidths are presented, with the analytical linewidths from Figure 3a used as the reference on the x-axis.

It is shown that, over the entire range, the non-thermal linewidth remains lower than the thermal linewidth and that the linewidth curves shift toward higher values as the temperature increases. This behavior provides further motivation for quantifying the ion temperature, as it modifies the cavity linewidth, which is highly sensitive to temperature-induced changes in the ion's motional state.

V. DETERMINATION OF ION TEMPERATURE AND AVERAGE PHONON NUMBER

We study the cavity-based EIT phenomenon with the motivation of determining the ion temperature. It is evident from section IV that the linewidth of the cavity-EIT spectrum appears to serve as a probe parameter for the trapped ion temperature. The ion temperature is incorporated in the systems by means of the thermal bath phonon occupancy (n_{th}) following Equation 4 and Equation 5 in steady-state.

The simulation is performed for four different

values of the thermal bath phonon occupancy, $n_{th} = 0.5, 1, 5, \text{ and } 10$, using the same set of parameters described in section III. A clear trend of increasing linewidth with increasing n_{th} is observed (see Figure 4a). This behavior indicates that the ion temperature can be mapped to the observed cavity-EIT linewidth. In other words, by analyzing the EIT width of the cavity-EIT spectrum, the ion temperature can be inferred. In the subsequent sections, we discuss the applicability of this technique over a wide range of experimental parameters that govern current and futuristic cavity-QED systems in the strong and weak coupling regimes.

In addition, the average phonon occupancy, \bar{n} , is an important quantity for various applications, such as estimating heating rates, determining fidelity of ion trap-based quantum gates, indicating the Lamb-Dicke regime etc. Since the phonon occupancy is directly related to temperature (see Equation 4), \bar{n} can also be estimated from the cavity-EIT linewidth.

We further perform simulations over a wide range of ion temperatures, from which the linewidth is calculated by fitting a Lorentzian function to the spectrum. The average phonon occupancy \bar{n} is extracted by taking the expect-

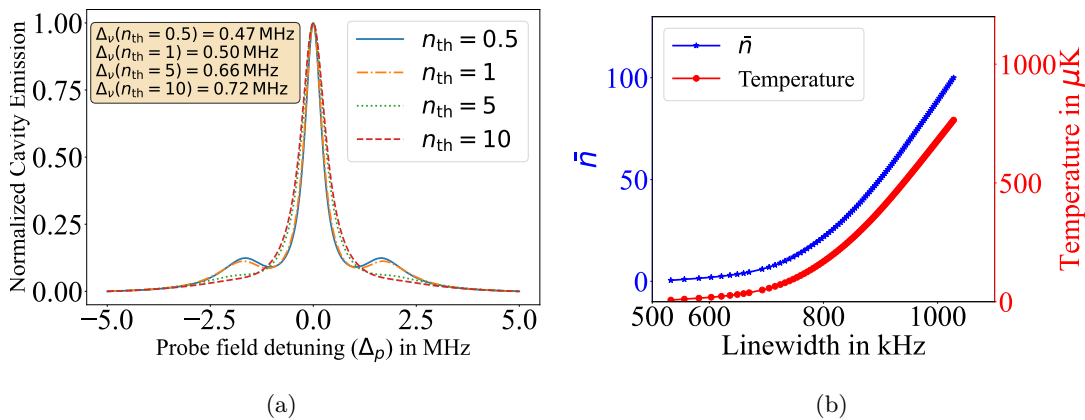


FIG. 4: (a) Cavity-EIT spectrum for different n_{th} value (b) Ion temperature and average phonon occupancy (\bar{n}) as a function of cavity-EIT linewidth. The cavity decay rate, $\kappa = 0.4\text{MHz}$, cavity coupling factor, $g = 3\kappa$. The decay rates from the excited states are taken as $\gamma_{eg} = \gamma_{eu} = \kappa$. The phonon coupling rate is taken as $\gamma_b = 0.25\kappa$.

tation over phonon number operator ($\langle b^\dagger b \rangle$). In Figure 4b, the ion temperature and \bar{n} are illustrated as functions of the cavity-EIT linewidth. The predicted temperature exhibits an asymptotic behavior at low linewidth values, indicating that at very low temperatures, variations in linewidth are minimal.

This behavior can be understood from the $\sqrt{\bar{n}}$ dependence of the control field Rabi frequency, Ω_c , which directly governs the cavity-EIT linewidth. At low temperatures, small changes in temperature lead to rapid variations in Ω_c , as described by Equation 1, resulting in noticeable changes in the linewidth. In contrast, at higher temperatures, the linewidth tends to saturate because variations in Ω_c become negligible.

The average phonon occupation, \bar{n} , follows a similar trend to the temperature as the cavity-EIT linewidth changes. This behavior arises from the approximately linear relationship between \bar{n} and temperature derived from Equation 4, given by

$$\bar{n} \approx \frac{k_B T}{\hbar \omega} \quad (9)$$

Further, we demonstrate how the ion-cavity coupling strength affects the cavity-EIT linewidth, g , and Rabi frequency of the coupling laser. We provide linewidth maps in two dimensions for a range of mean thermal phonon num-

ber values. Appendix C contains the relevant discussion and the requisite plots.

VI. THERMOMETRY OF A MULTI-ION CAVITY-QED SYSTEM IN THE WEAK COUPLING REGIME

The discussion so far has focused on a single ion confined in a high-finesse cavity and operating in the strong coupling regime. However, operating in the strong-coupling regime is experimentally challenging with only a single ion, requiring either a near concentric-cavity regime [42] or fiber cavities where the polished surfaces are placed very close to each other [43]. Interestingly, both of these configurations possess very small mode volumes leading to an increase in the single-atom cooperativity factor in a significant manner. Both regimes of operation are experimentally challenging, with substantial effort necessary in making and aligning cavity mirrors with very high reflectivity for the above two cavity configurations.

Our analysis reveals that it is possible to perform ion thermometry measurements for multi-ion cavity-QED systems having a relatively low single-ion cavity coupling factor ($g \ll \kappa, \gamma$) that places such systems in the weak coupling regime ($g \ll \kappa, \gamma$) for a single ion. We show through numerical simulations that it is possible to apply the proposed cavity EIT-based ion-thermometry

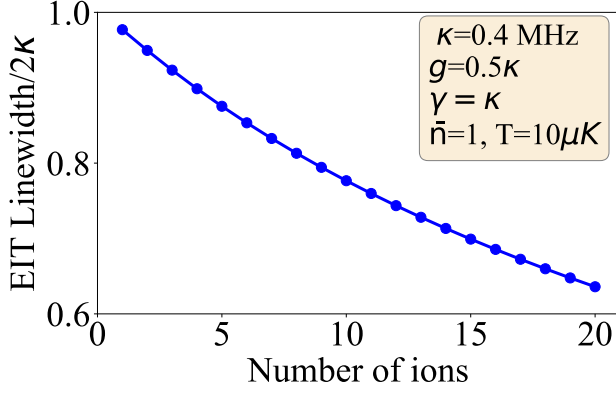


FIG. 5: Cavity-EIT linewidth variation with the number of ions. The simulation parameters are shown in the inset.

method discussed earlier even for such systems in the weak coupling regime, albeit using more than one ion coupled to the cavity mode instead of a single one. Using a multi-ion configuration coupled to the cavity mode places the system effectively in the strong coupling regime due to the collective ($g_{eff} \propto \sqrt{N}$) scaling up of the single-ion cavity coupling factor.

The Hamiltonian for a multi-ion cavity-QED system may be stated as

$$H = \Delta_p S_{gg} - \Delta_p a^\dagger a + g \left(a^\dagger S_{ge} + a S_{eg} \right) + \eta \Omega_c \left(S_{eu} b^\dagger + S_{ue} b \right) + \epsilon \left(a^\dagger + a \right). \quad (10)$$

where,

$$S_{ij} = \sum_{k=1}^{N_{\text{ion}}} |i\rangle^{(k)} \langle j|^{(k)} = \sum_{k=1}^{N_{\text{ion}}} \sigma_{ij}^{(k)}.$$

are the collective raising and lowering ionic operators for $i \neq j$, and ionic energy-level population operators for $i = j$.

The system dynamics, including the decoherence and dissipative effects, are determined by the master equation as,

$$\begin{aligned} \frac{d\rho}{dt} = & -i[H, \rho] + \kappa \left(2a\rho a^\dagger - a^\dagger a \rho - \rho a^\dagger a \right) \\ & + \gamma_{eu} \sum_{k=1}^{N_{\text{ion}}} \left(2\sigma_{ue}^{(k)} \rho \sigma_{eu}^{(k)} - \sigma_{ee}^{(k)} \rho - \rho \sigma_{ee}^{(k)} \right) \\ & + \gamma_{eg} \sum_{k=1}^{N_{\text{ion}}} \left(2\sigma_{ge}^{(k)} \rho \sigma_{eg}^{(k)} - \sigma_{ee}^{(k)} \rho - \rho \sigma_{ee}^{(k)} \right) \\ & + \gamma_{u,deph} \sum_{k=1}^{N_{\text{ion}}} \left(2\sigma_{uu}^{(k)} \rho \sigma_{uu}^{(k)} - \sigma_{uu}^{(k)} \rho - \rho \sigma_{uu}^{(k)} \right) \\ & + \gamma_b (n_{\text{th}} + 1) \left(2b\rho b^\dagger - b^\dagger b \rho - \rho b^\dagger b \right) \\ & + \gamma_b n_{\text{th}} \left(2b^\dagger \rho b - b b^\dagger \rho - \rho b b^\dagger \right). \end{aligned} \quad (11)$$

The method works as one may achieve the collective strong coupling regime with a larger number of ions coupled to the cavity mode, thanks to the scaling of the single-atom cavity coupling factor ($g_{eff} \propto \sqrt{N}$) g with ion number, N [44]. Here g is the single-ion cavity coupling factor. The dependence of ion number on cavity-EIT linewidth is depicted in Figure 5. As the ion number increases, the cavity-EIT linewidth decreases exponentially, making the EIT linewidth even narrower than the single-atom case in the strong coupling regime. It suggests that using a sufficient number of atoms/ions collectively coupled to the cavity, one may be able to realize a very narrow cavity-EIT linewidth, which might be useful for a variety of other applications as well, such as using them as reference transitions in atomic clocks, laser frequency stabilization, etc.

In the multi-atom/ion cavity system, the ion-cloud temperature may be estimated in a similar manner as outlined in the single-ion cavity EIT-based thermometry scheme as discussed in section V. We have shown the variation in temperature as a function of cavity-EIT linewidth in a fraction of empty cavity linewidth for different numbers of ions in Figure 6. The variation of the cavity EIT linewidth with temperature indicates that the linewidth is more sensitive to the temperature

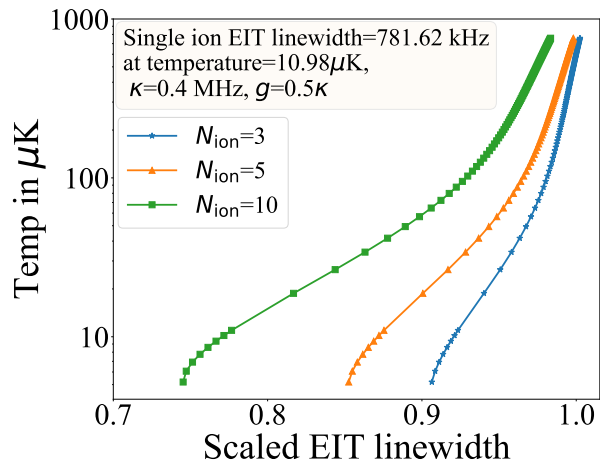


FIG. 6: Temperature vs cavity-EIT linewidth for multi-ions. The EIT linewidth is scaled with respect to the empty cavity width. The typical single-ion cavity EIT linewidth for one temperature is shown in the inset with the set of different parameters. Except for temperature, the same parameters have been chosen for the simulations performed in this plot.

as one considers a higher number of atoms/ions coupled to the cavity mode. Thus, the proposed thermometry method is particularly well-suited for cavity-QED systems with low ion-cavity coupling strength, especially when multiple ions are coupled to the cavity mode.

In the multi-ion model, we assume that all ions share an identical thermal occupation. This approximation is justified under a uniformly cooled condition, where all the ions are cooled to a sufficiently low temperature ($\approx 10 - 50 \mu K$) and undergo comparable coupling to the cavity field. Consequently, the collective cavity response can be described using a thermal distribution reminiscent of a single ion.

VII. THERMOMETRY OF A MULTI-ION CAVITY-QED SYSTEM WITH A LARGE EXCITED-STATE DECAY RATE

The three-level system we have considered for our ion thermometry is an ideal system, with a very low decay rate from the excited state. However, most ion species used in trapped-ion experiments have a broad excited-state linewidth (i.e.,

a large decay rate), which helps cool the ions efficiently with Doppler cooling.

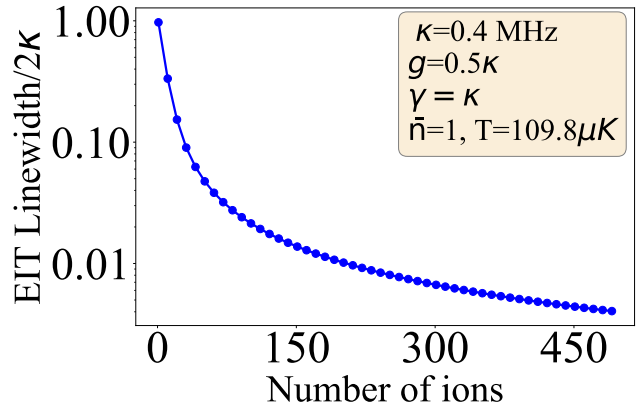


FIG. 7: Cavity-EIT linewidth variation with the number of ions for the case of high decay rate. The simulation parameters are shown in the inset.

A large decay rate induces decoherence in the system, which washes out the cavity-EIT effect, and only the bare cavity signal remains visible at the output. Several groups worldwide have demonstrated the cavity-EIT effect using ion/atom species with a large decay rate from the excited state [19, 44]. The experimental results from these systems show that for a single ion the cavity-EIT signal is not clearly visible; however, increasing the number of atoms leads to the appearance of cavity-EIT peaks. This occurs because, although the ion-cavity system is not configured in the strong coupling regime for a single ion/atom (as the decay rates exceed the cavity coupling factor), the effective coupling strength increases with multiple ions coupled to the intracavity field. Consequently, the collective ion-cavity coupling can overcome the large decay rates of the excited states, as discussed in section VI. More discussion about their system and an excellent agreement of our simulation results with the analytical expression and the reported experimental data can be found in Appendix A and B.

Motivated by these studies, we extend our ion-thermometry method to cases where the excited state decays rapidly to the ground states in a three-level lambda system. The cavity-EIT

peaks become visible when considering a multi-ion system, and the linewidth decreases with the increasing number of atoms, which is the usual behavior similar to that obtained in section VI. The variation of the cavity linewidth with the number of atoms, obtained from simulations performed for up to 500 ions, along with the corresponding simulation parameters, is depicted in Figure 7.

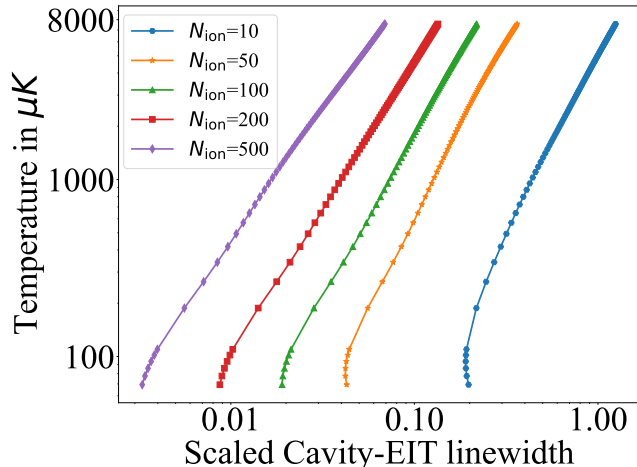


FIG. 8: Temperature vs linewidth for large decay from the excited level. For running the simulation, the cavity decay rate (κ) is taken as $0.4MHz$, whereas the cavity coupling factor is taken as $g = 3\kappa$. The decay rates from excited state $|e\rangle$ to $|u\rangle$ and $|g\rangle$ are $\gamma_{eu} = 20\kappa$, $\gamma_{eg} = 7\kappa$ respectively. The control field Rabi frequency is chosen as $\Omega_c = 2.5\kappa$, whereas the phonon coupling rate to the phonon bath is taken as $\gamma_b = 0.5\kappa$. The maximum probe field intensity (ϵ/κ) is taken as 0.01. Here, the cavity-EIT linewidth is scaled with respect to the empty cavity linewidth (2κ).

Interestingly, when running the simulations at different temperatures, i.e., for different values of n_{th} , the linewidth does not vary at all. This occurs because, for systems with large decay rates, the resolved sideband condition ($\gamma \ll \omega_{sec}$) is no longer satisfied. As a result, the motional sidebands cannot be resolved, which is essential for the thermometry process. Therefore, we conclude that, in addition to strong coupling, a necessary condition for implementing this thermometry method is that the ion must operate in the resolved sideband regime. The only remaining option in such cases

is to increase the trap frequency ω_c ; in other words, a tighter confinement of the ion with a deeper trapping potential is required.

To assess the applicability of the thermometry method in the presence of strong excited-state decay, we analyze the temperature dependence of the cavity-EIT linewidth for different numbers of ions as shown in Figure 8. A distinct and monotonic dependence of the normalized linewidth on the temperature is preserved even for large decay rates ($\gamma_{eu} = 20\kappa$, $\gamma_{eg} = 7\kappa$). Although the decoherence caused by spontaneous emission, which also partially broadens the EIT feature, collective enhancement ($g_{eff} \propto \sqrt{N}$) strengthens the effective light-matter interaction to compensate for decoherence. These results demonstrate that the suggested cavity-EIT thermometry method is robust even in regimes of significant radiative decay.

VIII. ROADMAP TOWARDS EXPERIMENTAL REALIZATION

We discuss an outline of experimental implementations for the trapped-ion thermometry method discussed in the previous sections of the article. As the thermal state detection method proposed is cavity EIT-based, one needs to engineer a trapped-ion cavity-QED system in the strong-coupling regime ($g^2 \gg \kappa\gamma$). This may be achieved in two ways. The first approach would be to engineer a cavity configuration in the near-concentric or near-confocal regime as per the requirements of the physics objectives. We recommend using a high finesse (> 50000) cavity, such that the coupling factor (g) is high enough to justify operation in the strong coupling regime ($g^2 \gg \kappa\gamma$) for a single atom/ion coupled to the cavity mode. The second approach focuses on a relatively relaxed regime of multi-ion based strong coupling regime of operation for a low-finesse cavity.

We need to choose a particular ion species with suitable energy levels, and appropriate ion trap parameters such that the system stays in the resolved sideband regime ($\gamma \ll \omega_{sec}$). Most of

the ion species used in cavity-QED experiments globally typically have strong dipole-allowed transitions, with broad linewidths, where sidebands are not resolved in general. Such traps operate with typical trap frequencies in the range (ω_{sec}) $\approx 0.5 - 2MHz$. So, one needs a judicious choice of the energy levels, such that the effective three-level system realized has very narrow linewidths for one of the excited levels.

One may also consider using a dipole allowed transition (where typical linewidths are in the range of $\approx 5 - 20MHz$) for the trapped ion strongly coupled to the cavity field, one should consider operating the ion trap in a very tight confinement (very deep trap potential) of the ion with secular frequency greater than the transition linewidth (Γ). Such a mode of ion trap operation has been experimentally validated [45], where an ${}^9\text{Be}^+$ ion was trapped with a very high RF voltage (600 V) and frequency (240 MHz), reaching secular frequencies in the range of $\sim 50 MHz$ and the sideband transitions were addressed in a dipole-allowed transition.

If one considers applying the proposed thermometry method with multiple ions in low-to medium-finesse (finesse values in the range 3000 – 15000) cavities having a relatively large mode waist (50–100 μm), about 10 ions coupled to the cavity mode can allow the system to operate in the strong-coupling regime, assuming a single ion cavity coupling factor of 0.5 MHz and cavity decay rate as well as the excited state decay rate of about 1 MHz.

IX. CONCLUSION

We have presented a cavity-assisted thermometry scheme for trapped ions that takes advantage of the dependence of cavity-induced EIT on ions' motional state. Through the explicit integration of thermalization and vibrational sidebands into a cavity-QED Λ -type system, we show that the mean phonon occupation and the ion temperature can be directly measured by the linewidth of the cavity-EIT transparency win-

dow. By means of motion-induced dephasing, thermal phonons perturb the coherence of the EIT dark state, resulting in a systematic expansion of the cavity-EIT resonance. This enables direct extraction of the ion temperature from the measured cavity transmission spectrum, eliminating the need for projective internal-state detection in Rabi spectroscopy. Overall, for the diagnosis of ion temperature in cavity-QED systems, cavity-EIT-based thermometry provides a minimally invasive and experimentally feasible method. The established coupling between ion motion and cavity transmission goes beyond thermometry, offering a platform to investigate measurement-induced effects in cavity-QED systems and enabling continuous monitoring of motional heating

Acknowledgments

Abhijit Kundu gratefully acknowledges financial support from IIT Tirupati, Government of India. Vijay Bhatt acknowledges support from the NQM (National Quantum Mission), Department of Science and Technology, Ministry of Science and Technology, Government of India through Project No. DST/QTC/NQM/QComm/2024/2(G) administered through the IITM CDOT SAMGYNA TECHNOLOGIES FOUNDATION, IIT Madras, Chennai, Tamil Nadu - 600113. Arijit Sharma acknowledges support from the NQM (National Quantum Mission), Department of Science and Technology, Ministry of Science and Technology, Government of India through Project Nos. DST/QTC/NQM/QComm/2024/2(G) and DST/QTC/NQM/QComm/2024/2(C) administered through the IITM CDOT SAMGYNA TECHNOLOGIES FOUNDATION, IIT Madras, Chennai, Tamil Nadu - 600113.

Conflicts of Interest

The authors declare no conflicts of interest.

-
- [1] D. Leibfried, R. Blatt, C. Monroe, and D. Wineland, Quantum dynamics of single trapped ions, *Rev. Mod. Phys.* **75**, 281 (2003).
- [2] H. Häffner, C. F. Roos, and R. Blatt, Quantum computing with trapped ions, *Phys. Rep.* **469**, 155 (2008).
- [3] C. Monroe and J. Kim, Scaling the ion trap quantum processor, *Science* **339**, 1164 (2013).
- [4] D. Fang, W.-B. Chen, C.-H. Zhang, J.-M. Cui, Y.-F. Huang, C.-F. Li, and G.-C. Guo, Cavity-assisted thermometry for a single trapped ion, *Phys. Rev. Appl.* **24**, 024037 (2025).
- [5] F. Diedrich, J. C. Bergquist, W. M. Itano, and D. J. Wineland, Laser cooling to the zero-point energy of motion, *Phys. Rev. Lett.* **62**, 403 (1989).
- [6] C. F. Roos, D. Leibfried, A. B. Mundt, F. Schmidt-Kaler, J. Eschner, and R. Blatt, Experimental demonstration of ground state laser cooling with electromagnetically induced transparency, *Phys. Rev. Lett.* **85**, 5547 (2000).
- [7] D. J. Wineland, C. Monroe, W. M. Itano, D. Leibfried, B. E. King, and D. M. Meekhof, Experimental issues in coherent quantum-state manipulation of trapped atomic ions, *J. Res. Natl. Inst. Stand. Technol.* **103**, 259 (1998).
- [8] M. Brownnutt, M. Kumph, P. Rabl, and R. Blatt, Ion-trap measurements of electric-field noise near surfaces, *Rev. Mod. Phys.* **87**, 1419 (2015).
- [9] D. M. Meekhof, C. Monroe, B. E. King, W. M. Itano, and D. J. Wineland, Generation of nonclassical motional states of a trapped atom, *Phys. Rev. Lett.* **76**, 1796 (1996).
- [10] C. Roos, T. Zeiger, H. Rohde, H. C. Nägerl, J. Eschner, D. Leibfried, F. Schmidt-Kaler, and R. Blatt, Quantum state engineering on an optical transition and decoherence in a paul trap, *Phys. Rev. Lett.* **83**, 4713 (1999).
- [11] A. J. Rasmusson, M. D'Onofrio, Y. Xie, J. Cui, and P. Richerme, Optimized pulsed sideband cooling and enhanced thermometry of trapped ions, *Phys. Rev. A* **104**, 043108 (2021).
- [12] I. Vybornyi, L. S. Dreissen, D. Kiesenhofer, H. Hainzer, M. Bock, T. Ollikainen, D. Vadlejš, C. F. Roos, T. E. Mehlstäubler, and K. Hammerer, Sideband thermometry of ion crystals, *PRX Quantum* **4**, 040346 (2023).
- [13] H. J. Kimble, Strong interactions of single atoms and photons in cavity QED, *Phys. Scr.* **1998**, 127 (1998).
- [14] M. Brune, F. Schmidt-Kaler, A. Maali, J. Dreyer, E. Hagley, J. Raimond, and S. Haroche, Quantum Rabi oscillation: a direct test of field quantization in a cavity, *Phys. Rev. Lett.* **76**, 1800 (1996).
- [15] A. Reiserer and G. Rempe, Cavity-based quantum networks with single atoms and optical photons, *Rev. Mod. Phys.* **87**, 1379 (2015).
- [16] V. M. Acosta, K. Jensen, C. Santori, D. Budker, and R. G. Beausoleil, Electromagnetically induced transparency in a diamond spin ensemble enables all-optical electromagnetic field sensing, *Phys. Rev. Lett.* **110**, 213605 (2013).
- [17] H. Wang, D. Goorskey, W. Burkett, and M. Xiao, Cavity-linewidth narrowing by means of electromagnetically induced transparency, *Opt. Lett.* **25**, 1732 (2000).
- [18] M. J. Werner and A. Imamoglu, Photon-photon interactions in cavity electromagnetically induced transparency, *Phys. Rev. A* **61**, 011801 (1999).
- [19] M. Mücke, E. Figueroa, J. Bochmann, C. Hahn, K. Murr, S. Ritter, C. J. Villas-Boas, and G. Rempe, Electromagnetically induced transparency with single atoms in a cavity, *Nature* **465**, 755 (2010).
- [20] H. Tanji-Suzuki, W. Chen, R. Landig, J. Simon, and V. Vuletić, Vacuum-induced transparency, *Science* **333**, 1266 (2011).
- [21] L.-M. Duan and C. Monroe, Colloquium: Quantum networks with trapped ions, *Rev. Mod. Phys.* **82**, 1209 (2010).
- [22] A. Reiserer, Colloquium: Cavity-enhanced quantum network nodes, *Rev. Mod. Phys.* **94**, 041003 (2022).
- [23] K.-J. Boller, A. Imamoglu, and S. E. Harris, Observation of electromagnetically induced transparency, *Phys. Rev. Lett.* **66**, 2593 (1991).
- [24] I. Novikova, R. L. Walsworth, and Y. Xiao, Electromagnetically induced transparency-based slow and stored light in warm atoms, *Laser Photonics Rev.* **6**, 333 (2012).
- [25] L. Ma, O. Slattery, and X. Tang, Optical quantum memory based on electromagnetically induced transparency, *J. Opt.* **19**, 043001 (2017).
- [26] G. Morigi, J. Eschner, and C. H. Keitel, Ground state laser cooling using electromagnetically induced transparency, *Phys. Rev. Lett.* **85**, 4458 (2000).
- [27] J. Souza, E. Figueroa, H. Chibani, C. Villas-Boas, and G. Rempe, Coherent control of quantum fluctuations using cavity electromagnetically induced transparency, *Phys. Rev. Lett.* **111**, 113602 (2013).
- [28] J. I. Cirac, R. Blatt, P. Zoller, and W. D. Phillips, Laser cooling of trapped ions in a standing wave, *Phys. Rev. A* **46**, 2668 (1992).
- [29] M. D. Lukin, M. Fleischhauer, M. O. Scully, and V. L. Velichansky, Intracavity electromagnetically induced transparency, *Opt. Lett.* **23**, 295 (1998).
- [30] H. Wu, J. Gea-Banacloche, and M. Xiao, Observation of intracavity electromagnetically induced transparency and polariton resonances in a doppler-broadened medium, *Phys. Rev. Lett.* **100**, 173602 (2008).
- [31] J. Zhang, G. Hernandez, and Y. Zhu, Slow light with cavity electromagnetically induced transparency, *Opt. Lett.* **33**, 46 (2007).
- [32] M. Albert, A. Dantan, and M. Drewsen, Cavity electromagnetically induced transparency and all-optical switching using ion coulomb crystals, *Nat. Photon.* **5**, 633 (2011).
- [33] Y.-C. Liu, B.-B. Li, and Y.-F. Xiao, Electromagnetically induced transparency in optical microcavities, *Nanophotonics* **6**, 789 (2017).
- [34] S. Zhang, Z.-P. Huang, T.-C. Tian, Z.-Y. Wu, J.-Q. Zhang, W.-S. Bao, and C. Guo, Sideband cooling of a trapped ion in strong sideband coupling regime, *Opt. Express* **31**, 44501 (2023).
- [35] D. Manzano, A short introduction to the Lindblad master equation, *AIP Adv.* **10**, 025106 (2020).
- [36] L. R. S. Santos, M. H. Oliveira, L. O. R. Solak, D. Z. Rossatto, and C. J. Villas-Boas, Fundamental limit to cavity linewidth narrowing with single atoms (2024), arXiv:2411.12422 [quant-ph].
- [37] M. Fleischhauer, A. Imamoglu, and J. P. Marangos, Electromagnetically induced transparency: Optics in coherent media, *Rev. Mod. Phys.* **77**, 633 (2005).

- [38] M. Lukin, Colloquium: Trapping and manipulating photon states in atomic ensembles, *Rev. Mod. Phys.* **75**, 457 (2003).
- [39] A. Dantan and M. Pinard, Quantum-state transfer between fields and atoms in electromagnetically induced transparency, *Physical Review A—Atomic, Molecular, and Optical Physics* **69**, 043810 (2004).
- [40] M. Mücke, E. Figueroa, J. Bochmann, C. Hahn, K. Murr, S. Ritter, C. J. Villas-Boas, and G. Rempe, Electromagnetically induced transparency with single atoms in a cavity, *Nature* **465**, 755 (2010).
- [41] M. Mücke, *Elektromagnetisch induzierte Transparenz mit einem einzelnen Atom*, Ph.D. thesis, Technische Universität München (2011).
- [42] J. Schupp, V. Krcmarsky, V. Krutyanskiy, M. Meraner, T. Northup, and B. Lanyon, Interface between trapped-ion qubits and traveling photons with close-to-optimal efficiency, *PRX Quantum* **2**, 020331 (2021).
- [43] H. Takahashi, E. Kassa, C. Christoforou, and M. Keller, Strong coupling of a single ion to an optical cavity, *Phys. Rev. Lett.* **124**, 013602 (2020).
- [44] M. Albert, J. P. Marler, P. F. Herskind, A. Dantan, and M. Drewsen, Collective strong coupling between ion coulomb crystals and an optical cavity field: Theory and experiment, *Phys. Rev. A* **85**, 023818 (2012).
- [45] S. R. Jefferts, C. Monroe, E. W. Bell, and D. J. Wineland, Coaxial-resonator-driven rf (Paul) trap for strong confinement, *Phys. Rev. A* **51**, 3112 (1995).
- [46] M. Albert, *A light-matter interface based on ion Coulomb crystals in an optical cavity*, Ph.D. thesis, Danish National Research Foundation, Center for Quantum Optics - QUANTOP, Department of Physics and Astronomy, The University of Aarhus (2010).
- [47] Q. A. Turchette, D. Kielpinski, B. E. King, D. Leibfried, D. M. Meekhof, C. J. Myatt, M. A. Rowe, C. A. Sackett, C. S. Wood, W. M. Itano, C. Monroe, and D. J. Wineland, Heating of trapped ions from the quantum ground state, *Phys. Rev. A* **61**, 063418 (2000).
- [48] E. Peik, J. Abel, T. Becker, J. von Zanthier, and H. Walther, Sideband cooling of ions in radio-frequency traps, *Phys. Rev. A* **60**, 439 (1999).

Appendix A: Transmission and reflection spectra with a bare cavity

To validate the theoretical model and numerical simulations discussed in the earlier sections of the article, we examine the empty-cavity limit by setting the ion-cavity coupling strength to zero and ignoring all phonon-related contributions in the Hamiltonian. Under these conditions, the system reduces to a driven, dissipative optical cavity described solely by the bare cavity Hamiltonian and the decay channels associated with it.

The Hamiltonian of the bare cavity system can

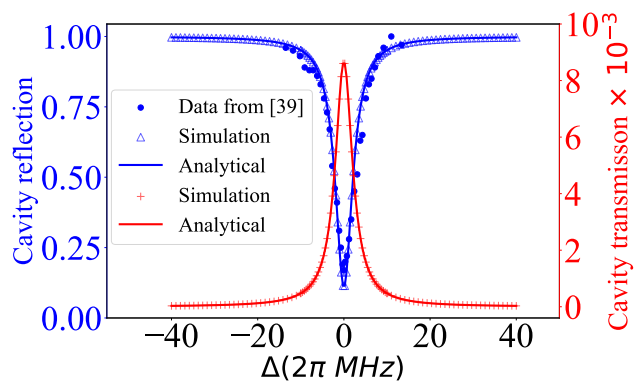


FIG. 9: Cavity reflection from simulation, analytical expression and published experimental data [46] as a function of probe detuning. The free spectral range of the cavity is $\nu_{FSR} = 12.7$ GHz. The transmission coefficients of the mirrors are $T_1 = 1500$ ppm and $T_2 = 5$ ppm, while the intracavity loss coefficient is $A = 600$ ppm. For these parameters, the resulting cavity finesse is approximately $F \sim 3000$.

be expressed as,

$$H_{\text{bare}} = \Delta_c a^\dagger a + i\sqrt{2\kappa_1}(a^\dagger a_{\text{in}} - a_{\text{in}}^\dagger a), \quad (\text{A1})$$

where a^\dagger (a) is the creation (annihilation) operator for the cavity mode, Δ_c represents the probe-cavity detuning, and a_{in} is the input field injected into the cavity.

Standard input-output relations are used to calculate the resulting transmission (\mathcal{T}) and reflection (\mathcal{R}) spectra. For an empty cavity, the response follows the well-known Lorentzian resonance profile determined by the cavity decay rates.

$$\mathcal{R} = \left| \frac{a_{\text{ref}}}{a_{\text{in}}} \right|^2 = \frac{(\kappa - 2\kappa_1)^2 + \Delta_c^2}{\kappa^2 + \Delta_c^2}, \quad (\text{A2})$$

$$\mathcal{T} = \left| \frac{a_{\text{trans}}}{a_{\text{in}}} \right|^2 = \frac{4\kappa_1\kappa_2}{\kappa^2 + \Delta_c^2}, \quad (\text{A3})$$

where, κ corresponds to the total decay rate of the cavity field, while κ_1 and κ_2 represent the contribution to the cavity loss arising from the imperfect reflectivity of the two cavity mirrors.

Figure 9 shows the cavity transmission and reflection spectra obtained from our numerical

simulation together with the corresponding analytical expression and previously reported experimental data [46]. The obtained spectra exhibit the expected Lorentzian lineshape with normalization, reproducing the well-known analytical response of a bare cavity. The validity of the reduced Hamiltonian reflecting the response of the bare cavity and the numerical method used throughout the manuscript are confirmed by the excellent agreement with the standard bare-cavity reflection and transmission profiles. The bare cavity response therefore serves as a baseline reference against which the modifications arising from ion-cavity interactions and phonon-induced effects can be reliably identified in the main results.

Appendix B: Comparison of simulation results with analytical expressions and experimental data

We verify our numerical simulations for a multi-ion cavity-QED system exhibiting a low single-ion cavity coupling factor as well as using ions with a large decay rate of the excited state. These systems can be driven in the collective strong coupling regime by appropriate choice of ions coupled to the cavity mode. We compare the simulated normalized cavity emission spectrum with previously published experimental data and results and compare them with available analytical expressions mentioned in [41, 46].

We first consider the cavity-EIT model described in [41], where a three-level Λ -type atom interacts with a single mode of an optical cavity. The atomic system consists of an excited state $|e\rangle$ and two long-lived ground states $|g\rangle$ and $|u\rangle$. The cavity mode is coupled to the transition $|g\rangle \leftrightarrow |e\rangle$ with coupling strength g while a classical control field with Rabi frequency Ω_c drives the transition $|u\rangle \leftrightarrow |e\rangle$. The cavity mode is driven by a weak probe field with amplitude ϵ and the cavity output spectrum is measured as a function of the probe-cavity detuning. In the rotating frame, the system Hamiltonian can be expressed as,

$$H = \hbar \left[\Delta_1 \sigma_{ee} + (\Delta_1 - \Delta_2) \sigma_{uu} + g(a^\dagger \sigma_{ge} + \sigma_{eg} a) + \frac{\Omega_c}{2} (\sigma_{ue} + \sigma_{eu}) + \epsilon(a^\dagger + a) - \Delta a^\dagger a \right], \quad (\text{B1})$$

where detunings are defined as $\Delta_1 = \omega_{eg} - \omega_p$, $\Delta_2 = \omega_{eu} - \omega_c$ and $\Delta = \omega_c - \omega_p$. ω_p and ω_c correspond to the probe and control field frequencies, respectively.

The intracavity photon number can be obtained analytically from the steady-state cavity field in the weak-probe limit as,

$$\langle n \rangle = \langle a^\dagger a \rangle = \frac{|\epsilon|^2}{|(\Delta + i\kappa) - \chi|^2}, \quad (\text{B2})$$

where κ represents the cavity decay rate and χ is the effective susceptibility of the EIT medium,

$$\chi = \frac{g^2 N (\Delta - \Delta_1 + \Delta_2 + i\gamma_{u,\text{deph}})}{(\Delta - \Delta_1 + i(\gamma_{eg} + \gamma_{eu}))} \times \frac{1}{(\Delta - \Delta_1 + \Delta_2 + i\gamma_{u,\text{deph}}) - \Omega_c^2/4}. \quad (\text{B3})$$

With these analytical expression and the parameters listed in [41] we compute the transmission spectrum and compared it with the outcomes of our numerical model. Figure 10 shows the normalized cavity emission as a function of probe detuning (Δ/κ) for $N_{ions} = 17$. As observed, the simulation accurately reproduces the key spectral features, including the central transparency peak and two sidebands.

The accuracy of the theoretical implementation is confirmed by the excellent agreement between the simulations and the analytical prediction. Furthermore, the close overlap with experimental data confirms the physical assumptions incorporated in the model. This agreement shows that the numerical framework reproduces experimentally observed behavior with high reliability and captures the cavity-EIT

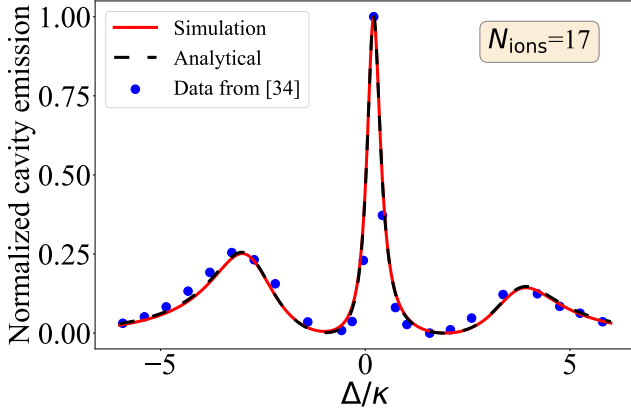


FIG. 10: Normalized cavity emission from simulation, analytical expression and published experimental data [41] as a function of probe detuning. The cavity decay rate (κ), is 1 MHz, while the single-atom cavity coupling rate (g_0) is 0.7κ . The control field Rabi frequency (Ω_c) is $3MHz$. The detuning for probe laser (Δ_1) and control laser (Δ_2) are 0.8κ and 0.55κ respectively.

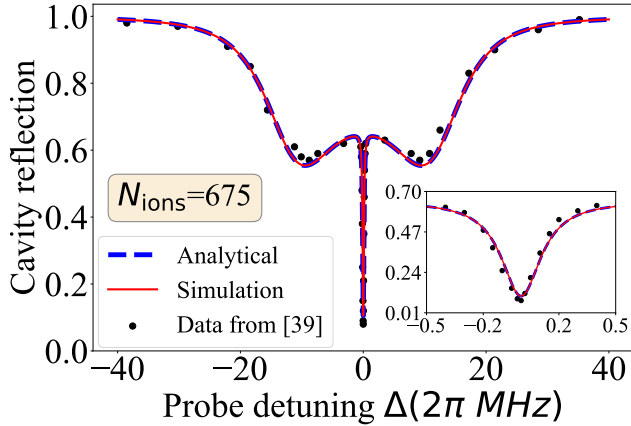


FIG. 11: Cavity reflection from simulation, analytical expression and published experimental data [46] as a function of probe detuning. The decay rate for 1st mirror (κ_1), 2nd mirror (κ_2) are $1.6MHz$ and $0.5kHz$ respectively. The decay rates from excited state to first and 2nd ground state are, $\gamma_{31} = 12.6 MHz$ and $\gamma_{21} = 0.6 kHz$ respectively. The single atom coupling factor $g = 0.48 MHz$, while control field Rabi frequency, $\Omega_c = 4.1 MHz$.

dynamics.

To further validate our numerical model, we also compare our results with the reflection spectra published in [46]. This work examines the cavity reflection from an ensemble of atoms coupled to the cavity mode in contrast to the

previous work in [41], which concentrates on the cavity transmission spectrum. Specifically, for the system of about 500 atoms, the reflection spectrum was investigated analytically and experimentally in [46].

The cavity-EIT spectrum shown in Figure 11 is deduced from the analytical expression of the normalized cavity reflectivity with respect to the input field, as explained in [46]. The reflectivity can be written as,

$$R = \left| \frac{a_{ref}}{a_{in}} \right|^2 = \frac{[\kappa_1 - \kappa_2 - \kappa_A - \text{Im}(\chi_\Lambda)]^2 + [\Delta - \text{Re}(\chi_\Lambda)]^2}{\kappa^2 + \Delta^2 + |\chi_\Lambda|^2 + 2[\kappa \text{Im}(\chi_\Lambda) - \Delta \text{Re}(\chi_\Lambda)]} \quad (\text{B4})$$

Here a_{ref} and a_{in} are the reflected and input field amplitude respectively. κ_1 , κ_2 and κ_A are the decay rates for field losses from the cavity first mirror, second mirror and additional internal losses due to various mechanisms. Δ is the probe field detuning and κ is the total decay rate ($\kappa = \kappa_1 + \kappa_2 + \kappa_A$). χ_Λ is the three-level non-linear susceptibility of the atomic ensemble, which can be expressed as,

$$\chi_\Lambda = \frac{ig^2N}{\gamma + i\Delta} \frac{\ln(1+s)}{s} \quad (\text{B5})$$

Where, g is the single ion coupling factor, N is the effective number of atoms coupled with the cavity field, γ is the combined decay rates for the excited state. The saturation parameter for the two-photon transition is s , which can be articulated as,

$$s = \frac{\Omega_c^2/2}{(\gamma_{12} + i\delta)(\gamma + i\Delta)} \quad (\text{B6})$$

Where, Ω_c , is the control field Rabi frequency, γ_{12} is the dephasing rate between the ground states. δ is the two-photon detuning, which is the difference between probe laser detuning (Δ) and control laser detuning (Δ_{32}), $\delta = \Delta - \Delta_{32}$.

Appendix C: Dependency of cavity-EIT linewidth on cavity coupling parameter g and control field Rabi frequency Ω_c for different n_{th}

A two-dimensional map of the cavity-EIT linewidth represented as the normalized full width at half maxima (FWHM) ratio as a function of the normalized control field Rabi frequency Ω_c and the normalized atom-cavity coupling strength g for various mean thermal phonon numbers n_{th} is shown in Figure 12. For a weakly excited motional state ($n_{th} = 0.5$) (see Figure 12a), the linewidth ratio remains close to unity over a large region of the parameter space. This suggests that thermal motion only slightly alters EIT coherence. As the value of thermal occupation increases $n_{th} = 1$ (see Figure 12b), a clear reduction of the FWHM ratio occurs, particularly in the regime of strong ion-cavity coupling and weak control fields. This reduction signals the onset of thermally induced decoherence. A higher phonon number ($n_{th} = 5, 10$) (see Figure 12c, Figure 12d) shows a more noticeable trend in which the parameter space is dominated by extended regions of reduced linewidth ratio. In this regime, thermal motion significantly perturbs the ion-cavity interaction, leading to enhanced dephasing and a degradation of the EIT interference. As the control-field strength increases, it partially mitigates this effect by stabilizing the dark state against motional fluctuations. The strong sensitivity of the cavity response to the ions' motional state is highlighted by the systematic and temperature-dependent modification of the cavity-EIT linewidth shown in these plots. This provides a solid foundation for thermometry using cavity-based EIT.

Appendix D: Verification of different sideband transition -related phenomenon

As proof of principle of our approach, we performed verification of different sideband transition related characteristics. In the case of sideband transitions, a two-level system dressed with vibrational levels is sufficient to address different properties. The sideband Hamiltonians used here are consistent with the Lamb-Dicke-

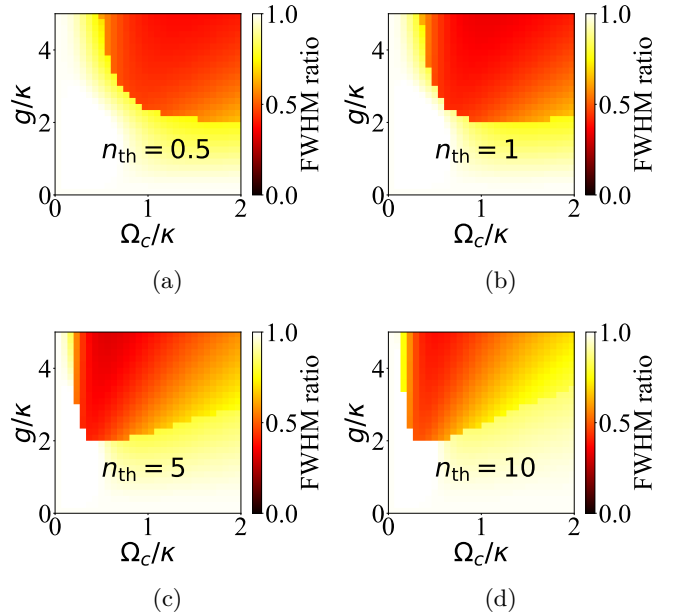


FIG. 12: Two-dimensional maps of the cavity-EIT linewidth as a function of the atom-cavity coupling strength g and the coupling-laser Rabi frequency Ω_c for different mean thermal phonon numbers n_{th} .

expanded interaction employed in the main text. The two kinds of sideband transitions (BSB and RSB) are described by the Hamiltonian which is similar to the 4th term (with the multiplication of the Lamb-Dicke parameter η) of Equation 10 with the reduced Hilbert space of only photon and phonon. The Hamiltonian for blue and red sideband transition can be written as [1],

$$\begin{aligned} H_{BSB} &= \eta\Omega_c (\sigma_{eu}b^\dagger + \sigma_{ue}b) \\ H_{RSB} &= \eta\Omega_c (\sigma_{eu}b + \sigma_{ue}b^\dagger) \end{aligned} \quad (D1)$$

For a thermal distribution of ion the strengths of red and blue sideband transitions are unequal and depends on the phonon number (n). The probability of occupying the excited state for RSB and BSB transition is related by the formula [47],

$$\frac{P_{RSB}}{P_{BSB}} = \frac{n}{n+1} \quad (D2)$$

We verified this principle for a range of phonon numbers and different Lamb-Dicke parameters. In Figure 13, the comparison between the probability ratio from simulation and phonon ratio

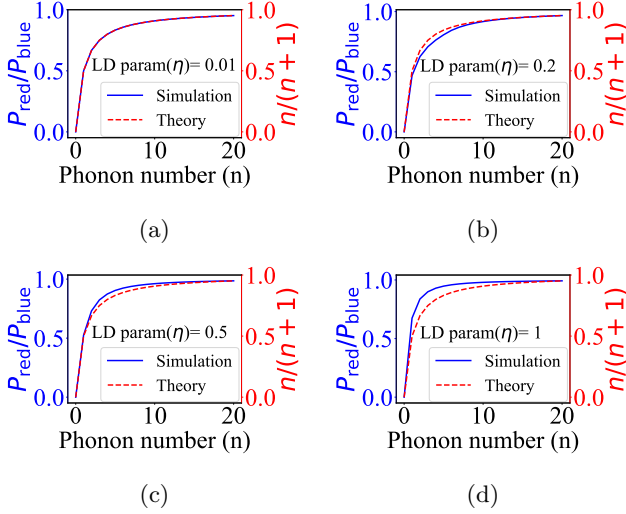


FIG. 13: Ratio of excited state occupation probability for blue and red sideband transition is compared with phonon number ratio. Plots (a)–(d) correspond to increasing values of the Lamb–Dicke parameter η .

from Equation D2 has been shown for four different Lamb-Dicke parameters. At lower values of Lamb-Dicke parameters, these two quantities are well-matched, which consistent with the theory. For higher Lamb-Dicke parameters the simulation result and theory start to deviate as the boundary of the Lamb-Dicke regime ($\eta \ll 1$) is approached, whereas sideband transitions assume that the ion is well within the Lamb-Dicke regime.

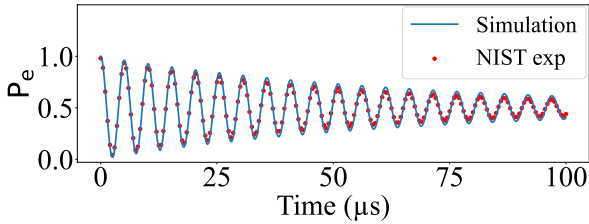


FIG. 14: Rabi oscillation in blue sideband transition for $n = 0 \rightarrow 1$. The red dots represent the data from the NIST experiment [9], and the solid blue curve represents the simulated result obtained using the same parameters as those employed in the experiment. The parameters are, $\eta = 0.202$, $\Omega = 2\pi \times 500$ kHz, $\gamma = 20$ kHz.

The dephasing and frequency in the Rabi oscillation of the blue sideband transition depend on the phonon occupation. There are many experimental verifications for this phenomenon [7, 9]. We have verified this argument, and it matches the experimental data reported in the NIST experiment (see Figure 14) [9]. A larger applica-

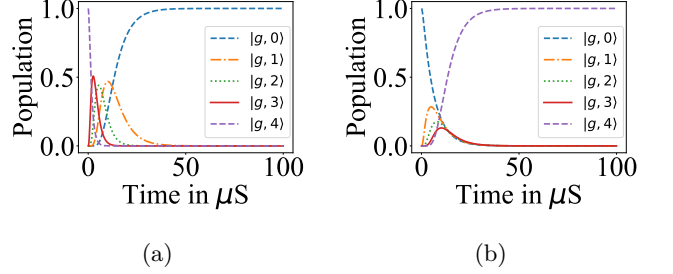


FIG. 15: Simulated state evolution with time. The simulation runs with Lamb-Dicke parameter, $\eta = 0.2$, Rabi frequency, $\Omega = 2MHz$, and excited state decay rate, $\gamma = 2\Omega$. (a) Time evolution of different states in red sideband transition. The initial state is taken as $|g, 5\rangle$, after applying sequential RSB pulses, phonon number decreases, and finally the system reaches the ground state, $|g, 0\rangle$. (b) Time evolution for blue sideband transition. population goes from initial $|g, 0\rangle$ to higher phonon state $|g, 5\rangle$.

tion of the sideband transition is the cooling of the atom to its motional ground state [5, 48]. When the resolved sideband regime is obtained ($\gamma \ll \omega_{sec}$) and the laser is tuned to a RSB transition, the atom loses one quanta of energy upon excitation ($|g, n\rangle \rightarrow |e, n-1\rangle$). From the excited state, there is a high chance that it spontaneously decays to the ground state with the same motional quanta ($|g, n-1\rangle$). Thus, a motional quanta has been reduced in this process. By repeating this process multiple times, the vibrational quanta has been reduced in each steps and eventually we reached to the ground state of the atom (see Figure 15a). Similarly, if the laser is tuned to the BSB transition, starting from a ground state, the atom lands in a higher phonon state depending on the number of sideband pulses applied (see Figure 15b).